Publications of the Astronomical Society of the Pacific, **117**:1271–1283, 2005 November
© 2005. The Astronomical Society of the Pacific. All rights reserved. Printed in U.S.A.

The VIMOS Integral Field Unit: Data-Reduction Methods and Quality Assessment

A. Zanichelli,[1] B. Garilli,[2] M. Scodeggio,[2] P. Franzetti,[2] D. Rizzo,[3] D. Maccagni,[2] R. Merighi,[4] J. P. Picat,[3] O. Le Fèvre,[5] S. Foucaud,[2] D. Bottini,[2] V. Le Brun,[5] R. Scaramella,[1] L. Tresse,[5] G. Vettolani,[1] C. Adami,[5] M. Arnaboldi,[6] S. Arnouts,[5] S. Bardelli,[4] M. Bolzonella,[7] A. Cappi,[4] S. Charlot,[8,9] P. Ciliegi,[4] T. Contini,[3] I. Gavignaud,[3,10] L. Guzzo,[11] O. Ilbert,[5] A. Iovino,[11] H. J. McCracken,[9,12] B. Marano,[7] C. Marinoni,[5] G. Mathez,[3] A. Mazure,[5] B. Meneux,[5] S. Paltani,[5] R. Pellò,[3] A. Pollo,[11] L. Pozzetti,[4] M. Radovich,[6] G. Zamorani,[4] and E. Zucca[4]

Received 2004 December 23; accepted 2005 August 3; published 2005 October 19

ABSTRACT. With the new generation of spectrographs, integral field spectroscopy is becoming a widely used observational technique. The Integral Field Unit (IFU) of the Visible Multi–Object Spectrograph (VIMOS) on the ESO VLT allows sampling of a field as large as $54'' \times 54''$, covered by 6400 fibers coupled with microlenses. We present here the methods of the data-processing software that has been developed to extract the astrophysical signal of faint sources from the VIMOS IFU observations. We focus on the treatment of the fiber-to-fiber relative transmission and the sky subtraction, and the dedicated tasks we have built to address the peculiarities and unprecedented complexity of the data set. We review the automated process we have developed under the VIPGI data organization and reduction environment (Scodeggio et al. 2005), along with the quality control performed to validate the process. The VIPGI IFU data-processing environment has been available to the scientific community to process VIMOS IFU data since 2003 November.

1. INTRODUCTION

Integral field spectroscopy (IFS) is one of the new frontiers of modern spectroscopy. Large, contiguous sky areas are observed to produce as many spectra as there are spatial resolution elements sampling the field of view. Integral field units (IFUs) use microlenses that are eventually coupled to fibers or all-reflective image slicers (Content et al. 2000; Prieto et al. 2000) to transform the two-dimensional field of view at the telescope focal plane into a long slit, or a set of long slits, at the entrance of the spectrograph. After the dispersing element, the contiguous spatial sampling and spectra produce a three-dimensional cube containing (α, δ) and λ information (see, e.g., Bacon et al. 1995, 2001; Allington-Smith & Content 1998; Allington-Smith et al. 2002).

The application of integral field spectroscopy to astrophysical studies may overcome many of the limitations posed by classical long-slit or multislit spectroscopy. It is particularly powerful for studying objects with complex two-dimensional distributions of the spectral quantity being measured. It offers a clear advantage over classical long-slit or multislit spectroscopy, because in one single observation it samples the object to be studied, regardless of complex shape, and because it collects all the emitted light (no slit losses). For instance, measuring the redshifts of galaxies in the core of distant clusters of galaxies is much more efficient with the IFS technique than with multislit spectrographs, because of the closely packed geometry of the core galaxies. IFS techniques are also a very powerful tool in the study of the internal dynamical structure of galaxies. Large-scale kinematical studies of galaxies were strongly limited by the insufficient spatial sampling of long-slit spectroscopy until the first studies with integral field spectrographs like TIGER (Bacon et al. 1995) appeared, followed by large samples of galaxies observed with SAURON (Bacon et al. 2001; Emsellem et al. 2004). IFUs are also well suited to observations of low surface brightness galaxies: the slit-loss problem faced by conventional spectrographs does not exist

[1] IRA-INAF, Via Gobetti, 101, I-40129 Bologna, Italy; a.zanichelli@ira.cnr.it.
[2] IASF-INAF, Via Bassini, 15, I-20133 Milano, Italy.
[3] Laboratoire d'Astrophysique de l'Observatoire Midi-Pyrénées (UMR 5572), 14, Avenue E. Belin, F31400 Toulouse, France.
[4] INAF-Osservatorio Astronomico di Bologna, Via Ranzani, 1, I-40127 Bologna, Italy.
[5] Laboratoire d'Astropysique de Marseille, UMR 6110 CNRS-Université de Provence, BP8, 13376 Marseille Cedex 12, France.
[6] INAF-Osservatorio Astronomico di Capodimonte, Via Moiariello, 16, I-80131 Napoli, Italy.
[7] Università di Bologna, Dipartimento di Astronomia, via Ranzani, 1, I-40127 Bologna, Italy.
[8] Max Planck Institut fur Astrophysik, 85741, Garching, Germany.
[9] Institut d'Astrophysique de Paris, UMR 7095, 98 bis Boulevard Arago, 75014 Paris, France.
[10] European Southern Observatory, Karl-Schwarzschild-Strasse 2, D-85748 Garching bei Munchen, Germany.
[11] INAF-Osservatorio Astronomico di Brera, Via Brera, 28, Milano, Italy.
[12] Observatoire de Paris, LERMA, 61 Avenue de l'Observatoire, 75014 Paris, France.

with IFUs, and such faint, extended objects are less difficult to detect.

The role of IFS is widely recognized today as a key technology to help solve some of the most fundamental questions of astrophysics, but dealing with the data obtained with integral field spectrographs is still a challenging task. On one hand, the reduction of data taken with fiber-based integral field spectrographs presents some peculiar aspects with respect to classical slit spectroscopy; for instance, variations in fiber-to-fiber relative transmission must be treated properly, and sky subtraction is a crucial step for many of these spectrographs. On the other hand, the huge amount of data obtained with even one night of observations using the new-generation integral field spectrographs, such as the VIMOS Integral Field Unit (Bonneville et al. 2003), makes manual data processing impossible. A new approach is required, based on the implementation of dedicated reduction techniques as part of an almost completely automated pipeline for data processing.

The Integral Field Unit of VIMOS is the largest IFS ever built on an 8 m class telescope. The high spectral multiplexing of VIMOS required the development of VIPGI, a semiautomatic interactive pipeline for data reduction (Scodeggio et al. 2005). The core reduction programs that constitute the main data-processing engine for the reduction of VIMOS data have been developed as part of a contract between the European Southern Observatory and the VIMOS Consortium. Such data-reduction software is now part of the online automatic pipeline for VIMOS data at ESO. With VIPGI we have kept the ability of these core reduction programs to perform fast reduction processes, but we have also added interactive tools that make it a careful and complete science reduction pipeline. VIPGI capabilities include dedicated plotting tools to check the quality and accuracy of the critical steps of data reduction, a user–friendly graphical interface, and an efficient data organizer. The VIPGI interactive pipeline has been available to the scientific community since 2003 November from the VIRMOS Consortium, to support observers through the data-reduction process.

In this paper we describe the peculiar aspects, principles of operation, and performance of the VIMOS IFU data-reduction pipeline implemented within VIPGI. In § 2 we describe the VIMOS IFU, and in § 3 we give the motivations leading to the development of a new, dedicated pipeline for VIMOS IFU data, while describing the general concepts of data analysis. Some aspects that are unique to VIMOS IFU data processing and analysis are discussed in more detail in §§ 4–8.2, together with examples of the results obtained.

2. THE VIMOS INTEGRAL FIELD UNIT

VIMOS (Visible Multi-Object Spectrograph) is a high-multiplexing spectrograph with imaging capabilities specifically designed to carry out survey work (Le Fèvre et al. 2002), that was installed on the third unit of the Very Large Telescope.

A detailed description of the VIMOS optical layout, and of the MOS observing mode in particular, can be found in Scodeggio et al. (2005). VIMOS's main features include the capability to simultaneously obtain up to 800 spectra in multislit mode and the availability of a microlens-fiber unit designed to perform integral field spectroscopy. To achieve the largest possible sky coverage, the VIMOS instrument has been split into four identical optical channels/quadrants, each acting as a classical focal reducer. When in MOS mode, each channel samples $\approx 7' \times 8'$ on the sky, with a pixel scale of $0''.205$ pixel^{-1}. The MOS and Integral Field Unit modes entirely share the four VIMOS optical channels. However, the VIMOS optical path in IFU mode differs from that of the MOS in three respects: the so-called IFU head, the fiber bundle, and the IFU masks.

The IFU head is placed on one side of the VIMOS focal plane (see Fig. 1 in Scodeggio et al. 2005) and consists of 6400 microlenses organized in an 80 × 80 array. Each microlens is coupled with an optical fiber. Spatial sampling is continuous, with the dead space between fibers below 10% of the fiber-to-fiber distance. The fiber bundle, which provides the optical link between the microlens array of the IFU head and the VIMOS focal plane, is first split into four parts, each feeding one channel, and then distributed over "pseudoslits" that are carved and properly spaced into four masks. Output microlenses on the pseudoslits restore the f/15 focal ratio needed as input to the spectrograph. The IFU masks are movable devices, and when the IFU observing mode is selected, they are inserted in the focal plane, replacing the MOS masks. The optical configuration of the IFU guarantees that field losses do not exceed 5%.

Figure 1 gives a schematic view of the IFU geometrical configuration. The microlens array of the IFU head, with a superimposed division of the fiber bundle into the four VIMOS quadrants/IFU masks, is detailed in Figure 1*a*. Fibers going to different pseudoslits that belong to the same IFU mask are grouped in sub-bundles, labeled A, B, C, and D. Each sub-bundle comprises five independent "modules" of 20 × 4 fibers; these are the "fundamental units" of the IFU bundle and are marked by different gray-scale levels. The 20 × 4 fibers in a module are rearranged to form a linear array of 80 fibers on a pseudoslit (see Fig. 1*b* for an example). Each pseudoslit holds five fiber modules. Figure 1*c* shows how the modules are organized over the pseudoslits in the case of the IFU mask corresponding to quadrant 3.

Contrary to what happens for MOS observations, the pseudoslit positions on the IFU masks are fixed. This produces a fixed geometry of the spectra on the four VIMOS CCDs (see Fig. 2 for an example). The information on the correspondence between the position of a fiber in the IFU head and the position of its spectrum on the detector is one of the fundamental ingredients of the data-reduction process, and together with other fiber characteristics, it is stored in the so-called IFU table (§ 3).

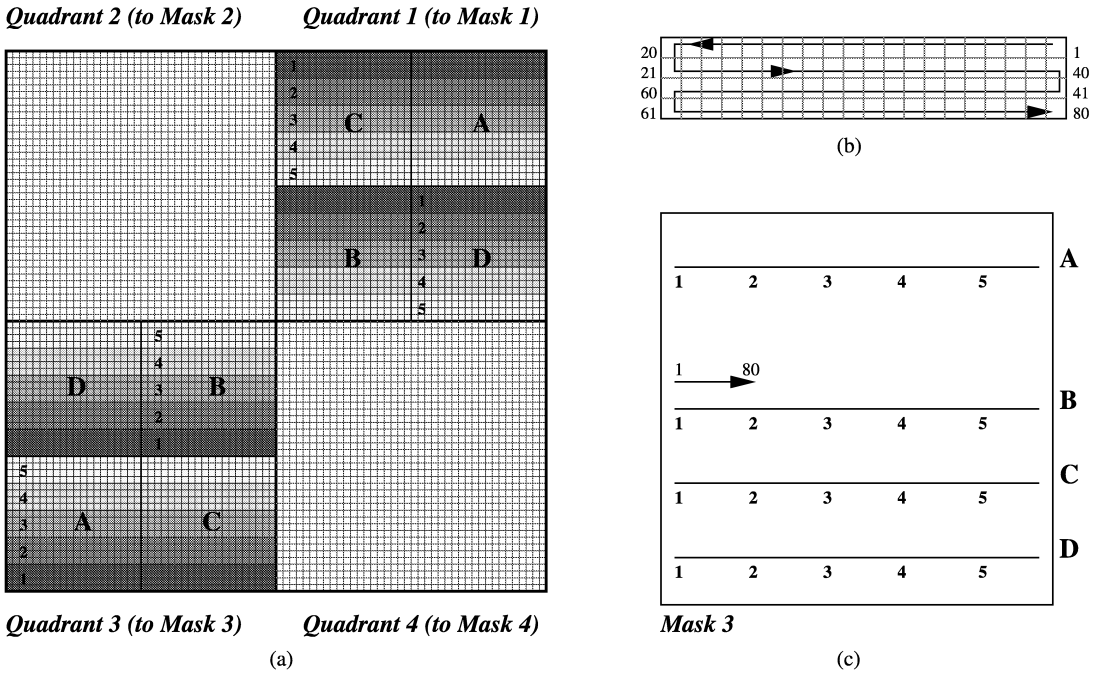

FIG. 1.—Geometrical layout of the VIMOS Integral Field Unit. (*a*) The 80 × 80 microlens array that forms the IFU head. Each quadrant is associated with a 1600 fiber bundle that conveys the collected light into one of the four VIMOS channels. For clarity, only details for quadrants 1 and 3 are shown. Sub-bundles group fibers associated with contiguous microlenses on each quadrant (the regions marked A, B, C, and D) and feed the four pseudoslits on the special IFU masks put in the VIMOS focal plane. A fiber sub-bundle is in turn divided into five modules of 80 fibers each. The fibers in each module are aligned onto the pseudoslits, according to a complex pattern, as can be seen in (*b*). Panel (*c*) illustrates how the fiber modules are organized over the pseudoslits in the case of the IFU mask 3.

IFU observations can be done with any of the available VIMOS grisms (see Table 1 in Scodeggio et al. 2005). At low spectral resolution ($R \sim 200$), four pseudoslits per quadrant provide 4 × 400 horizontally stacked spectra on each of the four VIMOS CCDs. The left panel of Figure 2 shows quadrant/CCD 3 in an IFU exposure taken with the low-resolution red grism; the four pseudoslits holding 400 spectra each are clearly visible. One of the fiber modules belonging to pseudoslit A is indicated with an arrow, and an enlargement of its 80 spectra can be seen in the right-hand panel. At high resolution ($R \approx 2500$), spectra span a much larger number of pixels in the wavelength direction over the CCDs, and only the central pseudoslit on each mask can be used. The complex rearrangement of fiber modules from the IFU head to the masks is such that the four central pseudoslits (marked B in Fig. 1) map exactly the central part of the field of view. This makes it possible to perform high spectral resolution observations while keeping the advantage of a contiguous field. A dedicated shutter is used to select only the central region of the IFU field of view.

Two different spatial resolutions, $0''.67$ and $0''.33$ fiber^{-1}, are possible, thanks to a removable focal elongator that can be placed in front of the IFU head. The higher spatial resolution translates to a smaller field of view. The sky area accessible to an IFU observation is thus a function of the chosen spectral and spatial samplings. Table 1 summarizes the values for the IFU field size as a function of the allowed spectral and spatial samplings.

3. THE IFU DATA REDUCTION

IFU data reduction is part of the VIMOS Interactive Pipeline and Graphical Interface (VIPGI). For a detailed description of the VIPGI functionality, as well as the handling and organization of VLT-VIMOS data, we refer the reader to Scodeggio et al. (2005).

The realization of a dedicated pipeline for the VIMOS IFU is mainly motivated by two considerations: (1) the need to be independent from already existing software environments (such as IRAF or IDL), which was (at that time) a general ESO requirement for VLT instrument data-reduction pipelines, and (2) some peculiarities of the instrument that required the development of specific processing tools. For example, the continuous coverage of the field of view does not guarantee the availability of permanently dedicated fibers for pure-sky observations during each exposure. A new tool for sky subtraction (§ 6) has been developed that does not require special observing

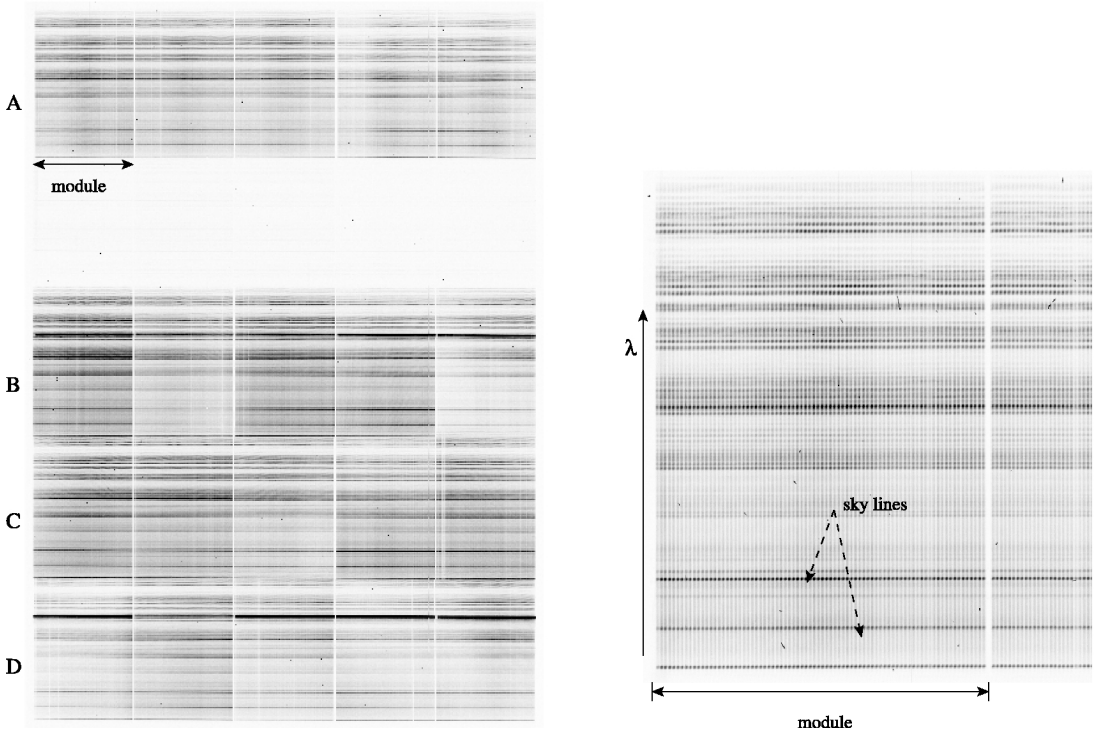

FIG. 2.—*Left*: Example of an IFU exposure. Only one of four quadrants is shown; the four pseudoslits with 400 spectra each are visible. Each spectrum spans 5 pixels in the spatial direction. One fiber module belonging to pseudoslit A is indicated in the left panel; an enlargement of the 80 spectra coming from this module is shown in the right panel.

techniques, such as "chopping," and thus does not impact the observing overhead.

As for MOS, the starting point for the reduction of IFU data is the knowledge of an instrument model (see § 4 in Scodeggio et al. 2005 for details); i.e., an optical distortion model, a curvature model, and a wavelength-dispersion solution. These models are periodically derived by the ESO VIMOS instrument scientists using calibration plan observations, and are stored in the image FITS headers as "first guess" polynomial coefficients. First-guess parameters are used as a starting point to refine the instrument model for scientific data. With such an approach, the best possible calibration is obtained for each individual VIMOS exposure. The refinement of first-guess models is a fundamental step in IFU data reduction, since the instrumental mechanical flexures are often a critical factor (see § 4.1).

With respect to hardware, each VIMOS quadrant is indeed a completely independent spectrograph, characterized by its own instrument model. For this reason, IFU data processing is performed on single frames; i.e., images from each quadrant are reduced separately until a set of fully calibrated one-dimensional reduced spectra are created. The final steps of data reduction, such as the creation of a two-dimensional reconstructed image or the combination of exposures in a jitter sequence (§ 8.2), are however performed only after all the images from all the quadrants have been reduced.

A high degree of automation is achieved by means of auxiliary tables used by the data-reduction procedures. In the case of the VIMOS IFU, fundamental information is listed in the IFU table. Starting from the instrument layout, this table gives the one-to-one correspondence between fiber position on the

TABLE 1
CHARACTERISTICS OF THE VIMOS INTEGRAL FIELD UNIT

Spectral Resolution	Field of View	Spatial Resolution (arcsec fiber^{-1})	Spatial Elements	Spectral Elements (pixels)
Low ($R \sim 200$)	54″ × 54″	0.67	6400	600
	27″ × 27″	0.33		
High ($R \sim 2500$)	27″ × 27″	0.67	1600	4096
	13″ × 13″	0.33		

IFU head and spectra on the CCD, as well as other fiber parameters, such as the relative transmission and the coefficients describing the fiber spatial profile (see discussion in § 6).

The first steps of IFU data reduction are the tracing of spectra on the CCD, cosmic-ray cleaning, and wavelength calibration—operations that lead to the extraction of two-dimensional spectra. Wavelength calibration is performed as it is for MOS, with an accuracy of the computed dispersion solution that is comparable to what is obtained for MOS spectra (see Scodeggio et al. 2005 for details). Extraction of one-dimensional spectra is generally done with the usual Horne (1986) extraction method, by means of spatial profiles determined for each fiber from the data alone. One-dimensional extracted spectra can be calibrated to correct for differences in fiber transmission and then properly combined to determine and subtract the sky spectrum. Flux calibration can be applied as a final step. If observations have been carried out using the shift-and-stare technique, one-dimensional reduced single spectra belonging to the same sequence can be corrected for fringing and properly combined in a data cube. Finally, a two-dimensional reconstructed image is built.

A block diagram of the operations performed by the VIMOS IFU data-reduction pipeline is shown in Figure 3. Optional steps are marked in italics. For instance, the removal of cosmic-ray hits, as well as relative transmission correction and sky subtraction, are not strictly needed in the reduction of short exposures of spectrophotometric standard stars. Moreover, sky subtraction may not satisfactorily work in the case of very crowded fields (see § 6) and can be skipped. Fringing correction is not necessary when the VIMOS blue grism is used, because its wavelength range is free from such an effect.

Key steps in the processing of VIMOS IFU data include the location of spectra on the CCDs, cosmic-ray cleaning, cross-talk contamination and relative transmission corrections, and sky subtraction. In the following sections, we focus our attention on these steps, to clarify their impact on the data-reduction process and motivate the need for dedicated reduction procedures, and also to describe the adopted methods and show the quality that is obtained.

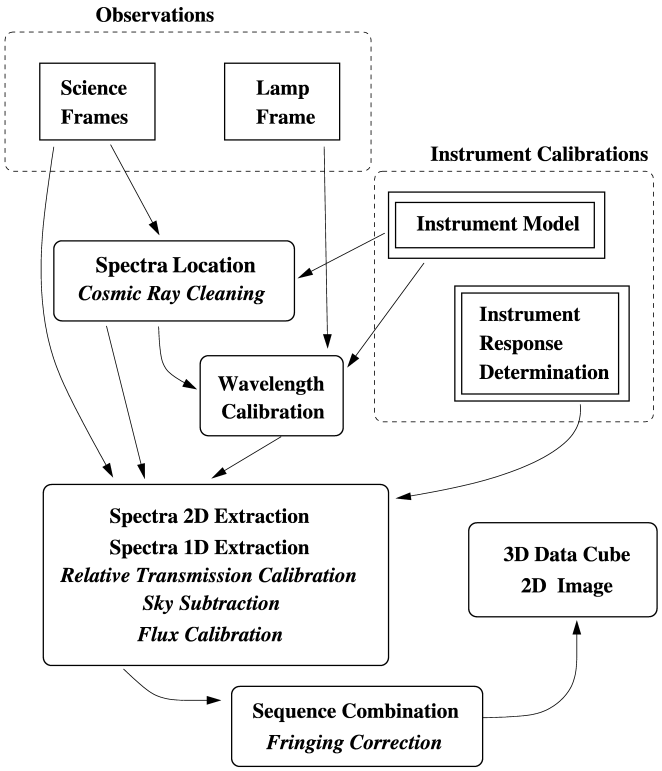

FIG. 3.—Block diagram showing the various steps of the reduction of VIMOS IFU data. Optional steps are marked in italics.

4. EXTRACTION OF VIMOS IFU SPECTRA

The extraction procedure consists of tracing spectra on the CCDs, applying wavelength calibration, and extracting two-dimensional and then one-dimensional spectra. The most critical aspects of spectral extraction are the accurate location of spectral positions on the detectors, and the cosmic-ray cleaning; the cross-talk effect is discussed in § 4.3.

4.1. Locating Spectra

When dealing with VIMOS IFU data, the location of spectra is a much more critical step than in multislit mode. This is a consequence of two instrumental characteristics of the VIMOS spectrograph: mechanical flexures and spectra distribution on the detectors.

As already discussed in § 2 of Scodeggio et al. (2005), the overall instrumental flexures induce image motion of the order of $\sim \pm 2$ pixels. In IFU mode, the additional and predominant sources of mechanical instability are the deployable IFU masks, and flexures are larger than in MOS mode. Shifts of the order of ± 5 pixels in the spectral positions between exposures taken at different rotation angles are typical, but values as large as 11 pixels have been observed. Such values are comparable to or larger than the spatial extent of a fiber spectrum on the VIMOS detectors (about 5 pixels) and are strongly dependent on the instrument rotator angle during the observations.

If shifts are comparable to the spatial size of a spectrum, it may become impossible to correctly determine the correspondence between a fiber on an IFU mask and its spectrum on the detector. As can be seen in Figure 2, the ~10 signal-free pixels between modules are easily identifiable regions, and a simple user interface allows one to set their (rough) position. Once an intermodule position is known, it is used as starting point from which, moving left and right, the positions of the 80 spectra belonging to adjacent modules can be measured. The spectral positions are traced with a typical uncertainty of 0.5 pixels. For each spectrum, a second-degree polynomial is fit to these

positions, and its coefficients are stored in the so-called extraction table, to be used for two-dimensional extraction. With respect to the instrument model coefficients, the extraction table gives a much more accurate description of the spectral location, since it is "tuned" to the data themselves.

The spectral location method for VIMOS IFU data has been extensively tested on data taken with the different grisms and has proven to be extremely robust in correctly identifying fibers and tracing spectra, irrespective of the amount of shift induced by flexures and/or distortions.

4.2. Cosmic-Ray Cleaning

Once spectra have been traced, and before the two-dimensional spectra are extracted, cleaning of cosmic-ray hits is performed. This reduction step is of great importance to good relative transmission calibration and sky spectrum determination, since the results of these tasks can be seriously affected by the presence of uncleaned cosmic rays that alter spectral intensities.

In principle, the best way to remove cosmic-ray hits would be to compare different exposures of the same field. However, two reasons forced us to develop an alternative method: first, in the case of the VIMOS IFU, image displacements due to mechanical flexures prevent the direct comparison of pixel intensities to remove cosmic-ray hits. Second, we were interested in having a method that would be general enough that it could also be applied to single exposures of bright objects. Taking into account these considerations, we developed an algorithm that works on single frames and whose principles of operation are also applicable to data taken with spectrographs other than VIMOS.

Compared to other existing tools for single-frame cosmic-ray removal (e.g., the COSMICRAYS routine in IRAF), the method implemented in the VIMOS IFU pipeline is different because it relies on the hypothesis that along the wavelength direction, spectra show a smooth behavior in their intensities. In the presence of emission lines or sky lines, their intensity *gradients* will be smooth enough to be distinguishable when compared with the abrupt changes generated by cosmic rays. This is shown in Figure 4, where the profile of a sky line obtained with the low-resolution blue grism is superimposed on the profile of a cosmic ray. Both profiles are cut along the wavelength direction.

Each IFU spectrum is traced along the CCD, column by column, and the intensity gradient array is computed and analyzed to search for sharp discontinuities. Intensity gradient arrays are inspected by sliding along them with a small "window" (of the order of 20 pixels in length) inside which the local mean and rms values are computed and used to discard discrepant gradient values, which are likely to be due to the presence of a cosmic ray. The median and rms are recomputed on the clipped gradient window data and used to build the actual upper and lower thresholds for cosmic-ray detection in the gradient window. The window size and number of σs used to compute thresholds are user-selected parameters.

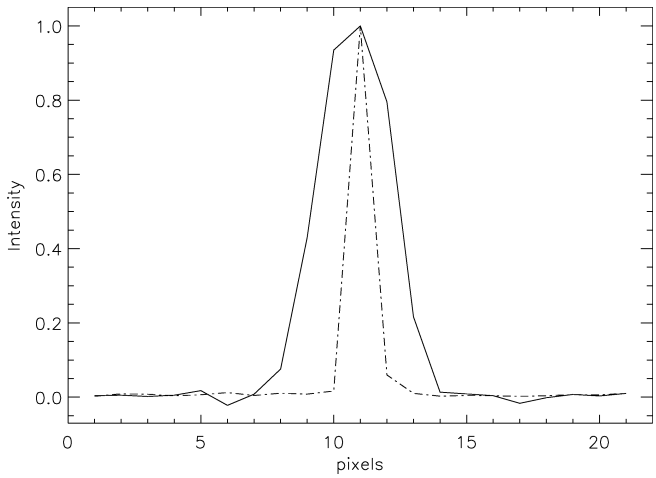

FIG. 4.—Sky line profile along the dispersion direction (*solid line*), superimposed on the profile of a cosmic ray (*dot-dashed line*).

Multiple-pixel hits are hard to distinguish from true emission lines. In an attempt to clean as many cosmic rays as possible without altering emission line shapes, we perform a further check before replacing the "suspect pixel value." The mean intensity in the local window is compared to the single-pixel intensities of the corresponding columns of the adjacent fibers. Because of the window dimensions (typically 20 pixels) over which the mean intensity is computed, such values should not be significantly different, except when an emission line is present. When a significant difference is found, this is interpreted as implying the presence of an emission line, and an average of the intensities in the two comparison spectra is used as a replacement value. On the other hand, if there is no difference, the intensity of pixels identified as cosmic rays is replaced by the local mean value.

Tests on spectra taken with the different VIMOS grisms showed that of all the pixels classified as cosmic-ray hits on the first pass, only about 0.3% actually belong to spectral lines. In these cases, the comparison with neighboring spectra has *not* confirmed the "cosmic-ray hypothesis," and data have not been incorrectly replaced.

It could be argued that emission lines from pointlike sources occupying only one fiber would be deleted by this method. In reality, given the median seeing in Paranal (0.″8) and the fiber dimension on the sky (0.″67), such an event would be extremely rare.

The cosmic-ray hits removal method implemented in the VIMOS IFU pipeline has been extensively tested and proved to be very efficient in cleaning both high and low spectral resolution data. On average, ~90% of the cosmic rays are removed: for cosmic-ray hits spanning 1–2 pixels, the removal

success rate is 99%, while more complex, extended hits are cleaned with a lower efficiency.

4.3. Cross-Talk

In building the VIMOS IFU, the main drivers were the size of the field of view and a high sky sampling. This resulted in a large number of spectra (400) lying along the 2048 CCD pixels. In this situation, in which each fiber projects onto five pixels on the CCD, neighboring spectra can contaminate each other, a phenomenon called "cross-talk."

The cross-talk correction must be based on the a priori knowledge of the fiber spatial profiles; i.e., the fiber analytic profile and its relevant parameters must be known from calibration measurements done in the laboratory on the fiber modules. For the VIMOS IFU, the fiber profiles are best described by the combination of three Gaussian functions, the first one modeling the core of the fiber, and the other two, symmetric with respect to the central one, modeling the wings. The positions and widths of the Gaussians can then be derived for each fiber by fitting the fiber profile to the data themselves, to get the best representation of the actual shapes and properly correct for cross-talk.

However, when applying a correction to data, the introduction of error is unavoidable. For the correction to be effective, this error must be noticeably smaller than the effect that is being corrected. In the case of cross-talk, this can only be achieved by having very good fits of the fiber profiles in the cross–dispersion direction, and we note that we have to fit a three-parameter function on a 5 pixel profile.

Simulations were performed to determine the maximum discrepancy between true and measured values of the shape parameters that still allows for a good correction of cross-talk. It has been found that fiber position uncertainties of about 0.5 pixels still guarantee that about $\frac{3}{4}$ of the fibers have an error in measured flux of less than 5%, while the most critical parameter is the profile width, which must be known with noticeably higher accuracy. The quality of cross-talk correction starts to worsen quickly when the maximum error on width measurement reaches an order of 0.2 pixels. In such a case, the number of fibers with a cross-talk correction accuracy worse than 5% rapidly becomes greater than 50% (see Fig. 5). Thus, at least concerning the profile width, these limiting uncertainties on the values of the profile parameters are of the same order of the accuracy we can achieve measuring these parameters from real data.

We then estimated the level of cross-talk present in the real data. It turned out that on average, ~5% of the flux of a fiber "contaminates" each neighboring fiber; i.e., by applying the correction procedure, the uncertainties we would introduce in IFU data would be of the same order of magnitude as the effect being corrected. For this reason, the cross-talk correction procedure is not currently implemented in the IFU data reduction.

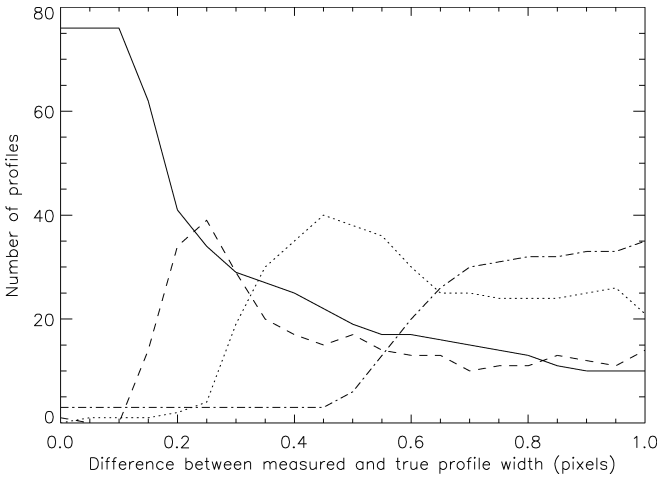

FIG. 5.—Performance of cross-talk correction as a function of the accuracy in the measurement of the fiber profile width. Lines show the number of fibers with an error on the recovered flux of less than 5% (*solid*), between 5% and 10% (*dashed*), between 10% and 20% (*dotted*), and greater than 20% (*dot-dashed*).

5. RELATIVE TRANSMISSION CORRECTION

Once one-dimensional spectra are traced and extracted from an IFU image, the next critical step is the correction for fiber relative transmission. Different fibers have different transmission efficiencies, and this effect alters the intensity of the spectra. This is exactly like the effect introduced by the pixel-to-pixel sensitivity variations in direct imaging observations, which require flat-fielding of the data.

The relative transmission calibration implemented in the VIMOS IFU pipeline consists of two steps, both executable at the user's discretion. The first step is the correction using "standard" relative transmission coefficients, which are provided by ESO as part of the instrument model calibrations and are usually determined from flat-field calibration frames. Such a standard correction cannot account for variations in relative transmission that may be due, for instance, to the fact that transmission degrades over time, or to variations in instrument position (e.g., rotator angle). For this reason, a second calibration step is performed: a "fine" relative transmission correction is executed on the scientific data themselves, based on the sky line flux determination described below. The two steps can be executed in sequence, the second one serving as a refinement of the relative transmission of the data themselves, or just one calibration step can be applied to the data. This choice guarantees a higher degree of flexibility in the data-reduction procedure, thus allowing the reducer to find the best solution for the data under consideration.

The correction for fiber relative transmission is derived by requiring that the flux of the sky lines must be constant in *all* fibers within one observation, and that there are no spatial variations inside the IFU field of view. The flux of a user-

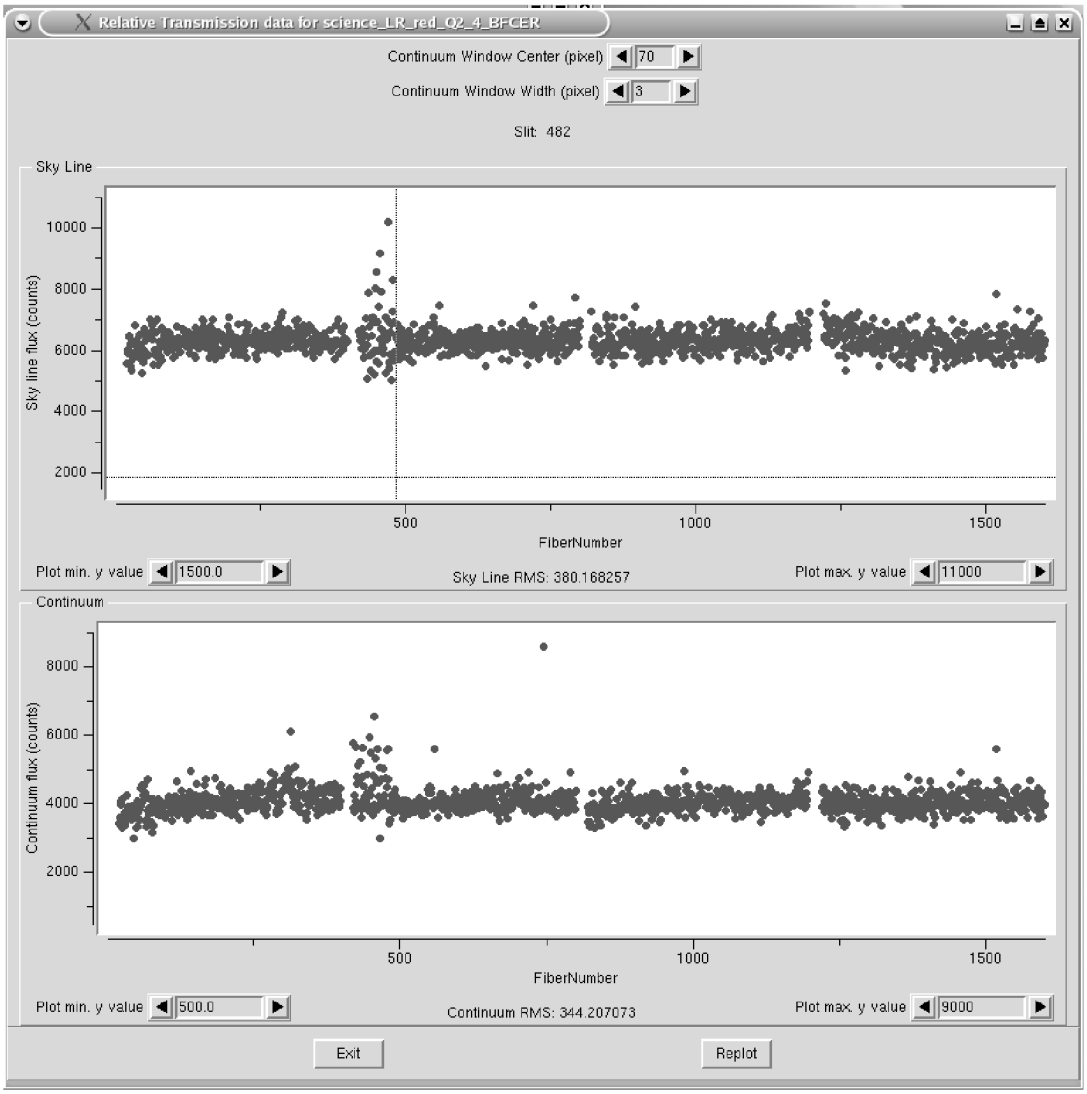

FIG. 6.—Graphical task for the analysis of the performance of relative transmission calibration for IFU data. *Top*: Intensity of the 1600 spectra at the wavelength of the sky line that has been used for the calibration (in this example, the 5892 Å line; spectra taken with low-resolution red grism). The bottom panel again shows the spectral intensity, this time computed in a user–selected continuum region at ~6000 Å. The rms of the intensities for each panel is also shown.

selected sky line is computed for each one-dimensional spectrum, a "relative transmission" normalization factor is determined with respect to a reference fiber, and it is finally applied to the one-dimensional spectra. Sky line flux can be determined by subtracting the contribution of the continuum from the line intensity: regions on both sides of the sky line are selected, and a second-order polynomial fit is done to obtain the best approximation of the continuum underlying the sky line. As noted below in § 6, the calibration of the fiber relative transmissions with the highest accuracy possible is of fundamental importance in order to obtain a good sky subtraction.

To minimize correction uncertainties, the sky line chosen for calibrating fine relative transmission coefficients should be characterized by a fairly stable flux and should be far from the regions affected by fringing. In the red domain, the 5892 Å sky line is usually a good choice (see Fig. 6 for an example). For data taken with the low-resolution blue grism, the 5577 Å sky line is a very good option.

The presence of uncleaned cosmic rays altering sky line intensities would lead to an overestimate of the fiber relative transmission, preventing a correct calibration. The presence of a cosmic-ray hit on a given sky line is extremely rare, however: for observations 45 minutes long, we statistically foresee that only ~6 spectra out of 1600 could be affected by this problem.

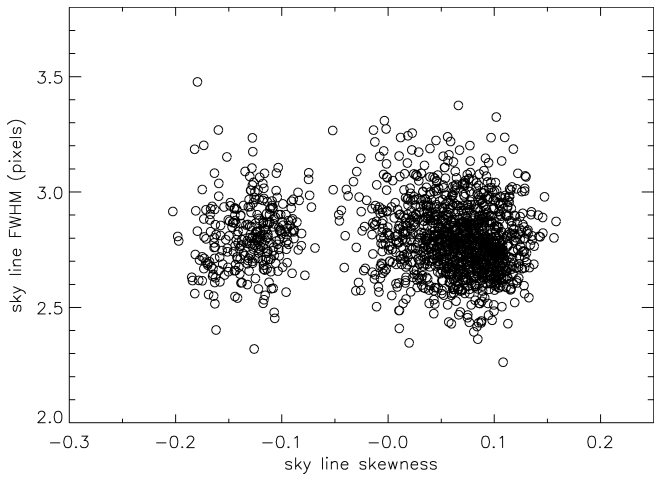

FIG. 7.—Distribution of the 5892 Å sky line skewness as a function of sky line width, measured for ~1600 one-dimensional spectra.

Even if the cosmic-ray removal algorithm failed to clean any of the hits on sky lines, it would still be a negligible fraction of spectra.

An interactive plotting task can be used to verify the results of relative transmission calibration by looking for residual trends in the data at a user-selected wavelength range in the spectra. An example of this task is given in Figure 6, which shows the results of applying the relative transmission calibration on an IFU exposure using the 5892 Å sky line. In the top panel, the intensity variations of the 5892 Å line in all 1600 spectra of the image are plotted, while the bottom graph shows the intensity of the continuum at ~6000 Å. Fibers 400–480 in Figure 6 belong to a module that is characterized by a very low transmission efficiency due to a nonoptimal assembly of the optical components. The low signal from these fibers translates to the determination of noisier relative transmission coefficients, and thus the visible scatter in their corrected intensities.

The relative transmission calibration procedure currently implemented in the VIPGI pipeline guarantees excellent results, with differences in the corrected intensities within 5%–7% over all modules.

6. SKY SUBTRACTION

Due to its design, the VIMOS IFU does not have "sky-dedicated fibers"; that is, fibers that are a priori known to fall on the sky. Moreover, once the light enters an optical fiber, the information on its spatial distribution is lost: individual fiber spectra on the CCD do not show regions with either pure sky emission or object signal, as happens in slit spectroscopy. Therefore, the determination of the sky spectrum to be subtracted from the data, which is an optional operation, cannot be done in the same way as it is for classical spectroscopic data reduction.

IFU spectra can include either the superposition of sky background and astronomical object contribution, or pure sky background. In those cases in which the field of view is relatively empty (i.e., when at least half of the fibers do not fall on an object), sky spectrum determination can be achieved by properly selecting and combining spectra that are likely to contain pure sky signal. These spectra can be selected using the histogram of the total intensities: each spectrum is integrated along the wavelength direction, and the total flux distribution is built. In a "mostly empty field," such a distribution will show a peak due to pure sky spectra, plus a tail at higher intensities where object+sky spectra show up. Spectra whose integrated intensity is inside a user-selected range around the peak will be pure sky spectra. A median combination of such spectra will ensure that any residual contamination by faint objects is washed out.

The sky-subtraction method implemented in the VIPGI pipeline for IFU data gives good results on deep survey observations of fields devoid of extended objects, but of course it is less optimal for observations of large galaxies covering the entire field of view.

The physical characteristics of the IFU fiber/lenslet system, together with the resampling executed on two-dimensional spectra for wavelength calibration, account for the fact that different fiber spectra are described by different profile shape parameters, such as FWHM and skewness. Along the wavelength direction, this is reflected in different shapes of the spectral lines. Such an effect, if not properly taken into account, affects the quality of sky subtraction: combining spectra with different line profiles would lead to an "average" sky spectrum whose line profiles do not match any of the original spectra, and subtracting this sky spectrum from the data would result in the presence of strong S-shaped residuals.

We performed many tests on real data to determine the relevant profile parameters: grouping spectra according to the line FWHM value does not seem to have any influence on the goodness of sky subtraction (i.e., on the strength of the S-shaped residuals). In Figure 7 the skewness of the 5892 Å sky line is plotted as a function of line width for ~1600 spectra. It can be seen that the distribution of line widths is pretty normal, and its relatively small dispersion makes it an unimportant parameter in the line profile description. However, Figure 7 shows a very clear bimodality in the distribution of line skewness. Such bimodality is surely an artifact that is derived from the undersampling of the line profile: with a typical FWHM of ~3–4 pixels, we can only see whether skewness is positive or negative. Nevertheless, our tests have shown that grouping fibers according to the sign of their skewness does indeed influence the strength of residuals. A further classification according to other line shape parameters would lead to too many fiber groups, each with too few spectra to allow for a robust sky determination. Finally, a line's shape changes

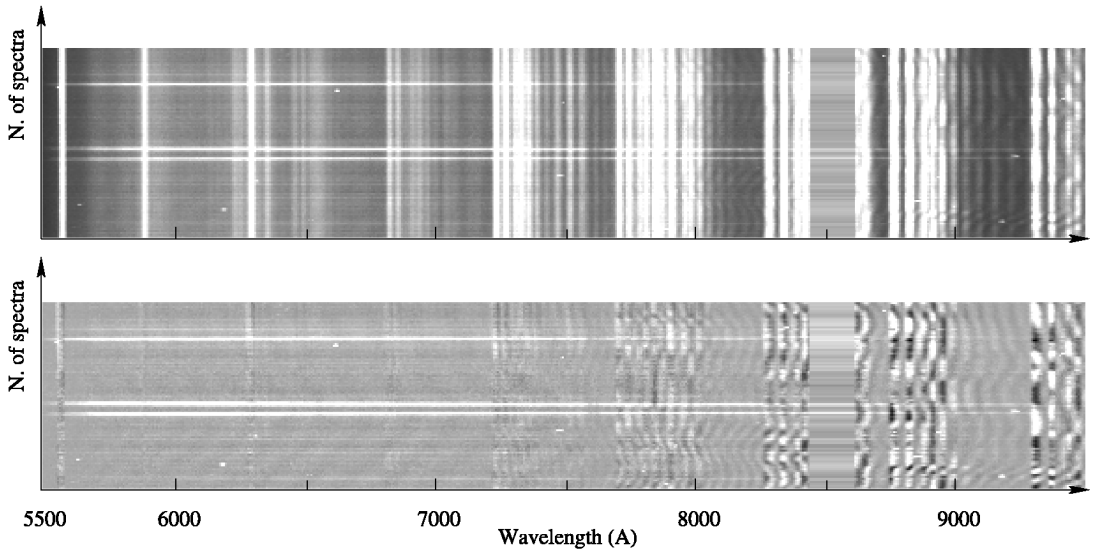

FIG. 8.—Example of the results obtained by the sky subtraction procedure. *Top*: One-dimensional relative transmission–corrected spectra in an exposure taken with the low-resolution red grism. *Bottom*: Same spectra after sky subtraction. The 5892 Å sky line has been used to group spectra before "average" sky spectrum computation. In the ~8500 Å region, the zero order due to a nearby pseudoslit has been clipped, creating a "flat" intensity distribution.

across the focal plane, due to the dependence of the instrument focus and optical aberrations on the distance from the instrument (in the case of VIMOS, the quadrant) optical axis. For this reason, we separately analyze spectra from different pseudoslits. Thus, sky subtraction first consists of grouping spectra according to the skewness of a user-selected sky line. Then for spectra belonging to each skewness group, the distribution of total intensities is built. Finally, an "average" sky spectrum is computed and subtracted from all the spectra belonging to that group.

Given the adopted method for sky subtraction, an overall good relative transmission calibration is essential to get a correct intensity distribution and thus a proper selection of pure sky spectra. On the other hand, due to the median combination, if just one or a few spectra have not been perfectly corrected for fiber relative transmission, it will not affect sky subtraction. The sky subtraction procedure guarantees good results, with the mean level over the continuum well centered around 0 in spectra where no object signal is present, and an rms of the order of a few percent. An example of sky-subtracted spectra can be seen in Figure 8.

7. FLUX CALIBRATION

The last step of data reduction on single observations is flux calibration, done in a standard way by multiplying one-dimensional spectra by the sensitivity function derived from standard-star observations. All the spectra containing flux from the standard star are summed together, and the instrumental sensitivity function is computed from comparisons with the real standard-star spectrum from the literature.

On the basis of a few objects with known magnitudes that have been observed with the VIMOS IFU, we have estimated that the overall absolute flux accuracy that can be reached with good-quality spectrophotometric calibrations is of the order of 15%, given the unavoidable sources of uncertainty, such as cross-talk contribution (of the order of 5%), relative transmission correction (between 5% and 10%), and sky subtraction (a few percent).

8. FINAL STEPS: JITTER SEQUENCES DATA REDUCTION

The final result of the single-frame reduction procedure is a FITS image containing intermediate products of the reduction (e.g., spectra not corrected for fiber transmission, or not sky subtracted) in the form of image extensions, plus some tables created and/or used during the execution of the different tasks.

In many cases, observations had been carried out using a jittering technique (the telescope is slightly offset from one exposure to the next). In these cases, the spectra from the single exposures must be stacked together according to their offsets, and in this process, correction for fringing can also be applied.

8.1. Correcting for Fringing

Due to the characteristics of the VIMOS CCDs, when observing in the red wavelength domain, one has to deal with the fringing phenomenon, whose effects show up at wavelengths larger than ~8200 Å in VIMOS spectra.

The decision to carry out fringing correction at the stage of stacking the single exposures is dictated by the consideration

that during a typical jitter sequence (a few hours' exposure time), the fringing pattern remains relatively constant. On the other hand, the overall background intensity and the relative strength of the individual sky emission lines can vary significantly over the same timescales. Likewise, the physical location of the spectra on the CCD changes because of flexures (see § 4.1 for an evaluation of flexure-induced image motions). Our approach has been to correct first for the most rapidly changing effects (first spectral location, then sky background) and only in the end to try to correct for fringing, which correction is then computed and applied to one-dimensional extracted spectra that have already been corrected for cosmic-ray hits, relative fiber transmission, etc.

The fringing correction can only be applied to jittered observations and is performed separately for the sets of images coming from different quadrants. First, all the spectra obtained in the jitter sequence for a given fiber are combined, without taking into account telescope offsets: any object signal is thus averaged out in the combination, and what remains is a good representation of the fringing pattern, which is then subtracted from each single spectrum.

The quality of fringing correction is very good. Figure 9 shows a result of the reduction of a sequence of nine jittered exposures of the Chandra Deep Field South. Observations were done using the low-resolution red grism (wavelength range 5500–9500 Å, dispersion 7.14 Å pixel^{-1}), with single-frame exposure times of 26 minutes. In Figure 9 (*top*), the exposures have been combined without applying any correction for fringing, while the bottom panel shows the result after having corrected for fringing as explained above. It can be seen that fringing correction is efficient in almost completely removing the residuals in the $\lambda > 8200$ Å region of the spectra.

8.2. Stacking Jittered Sequences of Exposures

Stacking is done all at once using all the available images from the VIMOS quadrants. In fact, due to the contiguous field of view of the VIMOS IFU, and given the arrangement of fibers on the four VIMOS quadrants, an object spectrum can "move" from one quadrant to the other, going from one jittered exposure to the next.

Image stacking makes use of data cubes, i.e., three-dimensional images in which the (x, y) axes sample the spatial coordinates, and the z-axis samples the wavelength. One data cube is created, from the four images of each IFU exposure. Jitter offsets are computed by using the header information on the telescope pointing coordinates, or by means of a user-given offset list, which is used to build a final three-dimensional image, starting from single data cubes. Variations of the relative transmission from quadrant to quadrant, and inside the same quadrant from one exposure to the next one in the sequence, are accounted for by properly rescaling image intensities.

The output of the reduction procedure is a FITS image containing all the stacked one-dimensional spectra in the final data cube. Each spectrum is written in a row of the output image (see Fig. 9), and a correspondence table between the position of the spectrum in the final three-dimensional cube is appended to it.

Finally, a two-dimensional reconstructed image can be built for scientific analysis. In Figure 10 we show an example of a two-dimensional reconstructed image from VIMOS IFU observations of the candidate cluster MRC 1022–299, associated with a high-redshift radio galaxy (McCarthy et al. 1996; Chapman et al. 2000). A sequence of five jittered exposures of 26 minutes each, taken with the low-resolution red grism, has been combined and integrated over the wavelength range 5800–8000 Å (Fig. 10, *left*) and over a narrowband 100 Å wide centered at 7100 Å (*right*), where an emission line identified with O II is observed in the radio galaxy spectrum. The radio galaxy, which is invisible in the broadband image, shows up at the center of the field in the narrowband image. From the O II line, we got a redshift of 0.9085 for the radio galaxy, consistent with the value quoted by McCarthy et al. (1996).

Two-dimensional reconstructed images can be built from any kind of one-dimensional extracted spectra (e.g., transmission-corrected or sky-subtracted ones) by using the sky-to-CCD fiber correspondence given in the standard IFU table, or in the case of a jitter sequence reduction, in the associated correspondence table. These images are particularly useful when dealing with crowded field data, when the automatic sky subtraction recipe cannot guarantee good results. In such cases, the reduction to one-dimensional spectra can be done without sky subtraction. A preliminary two-dimensional image can be reconstructed and used to interactively identify fibers/spectra in object-free regions, which can later be combined to obtain an accurate estimate of the sky background signal.

9. SUMMARY

The VIMOS Integral Field Spectrograph has required a new approach for processing the large amount of data produced by 6400 microlenses and fibers.

The instrumental IFU setup and the arrangement of spectra on the four VIMOS detectors have motivated the development of dedicated recipes, with the possibility of carefully checking the quality of results by means of interactive tasks.

With the large number of spectra acquired by the VIMOS IFU, it has been necessary to implement IFU data processing in a pipeline scheme that is as automated as possible. VIMOS IFU data processing is implemented under the VIPGI environment (Scodeggio et al. 2005) and has been available to the scientific community to process VIMOS IFU data since 2003 November.

We have estimated that the overall absolute flux accuracy that can be reached with our pipeline is of the order of 15%, the main sources of uncertainty being the cross-talk contribution (significant, of the order of 5%), the relative transmission correction (between 5% and 10%), and sky subtraction (a few percent).

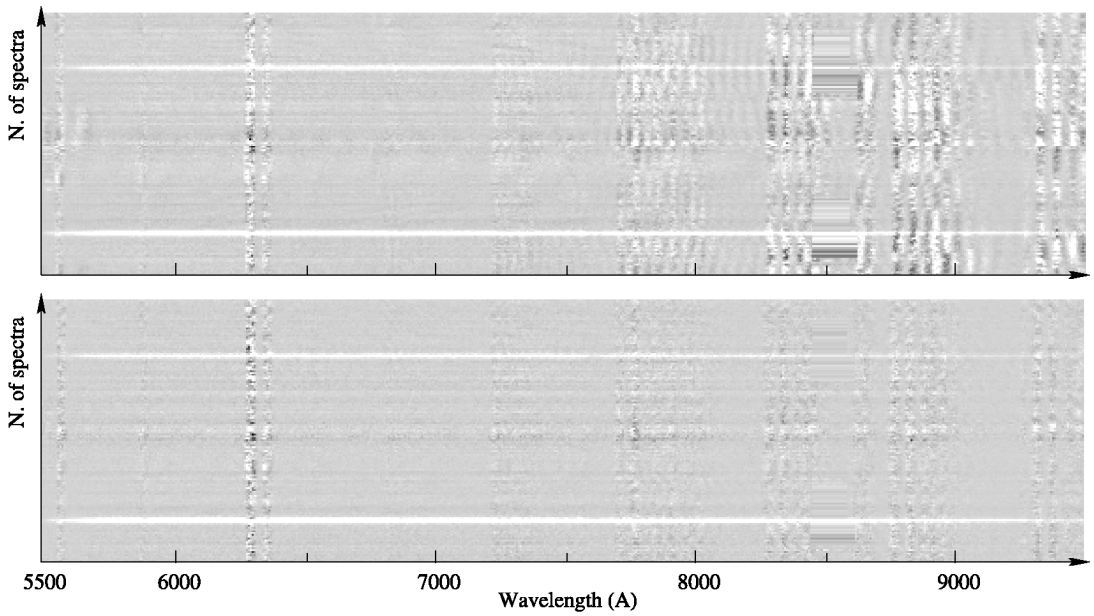

FIG. 9.—Efficiency of fringing correction: an example of jitter–combined fully reduced sequence of nine exposures, 26 minutes each, taken with the low-resolution red grism (wavelength range 5500–9500 Å) of the Chandra Deep Field South. Each row shows a different spectrum. Top and bottom panels respectively show data without and with the application of fringing correction. As can be seen in the bottom panel, at wavelengths larger than ~8200 Å, very low fringing residuals are left after correction.

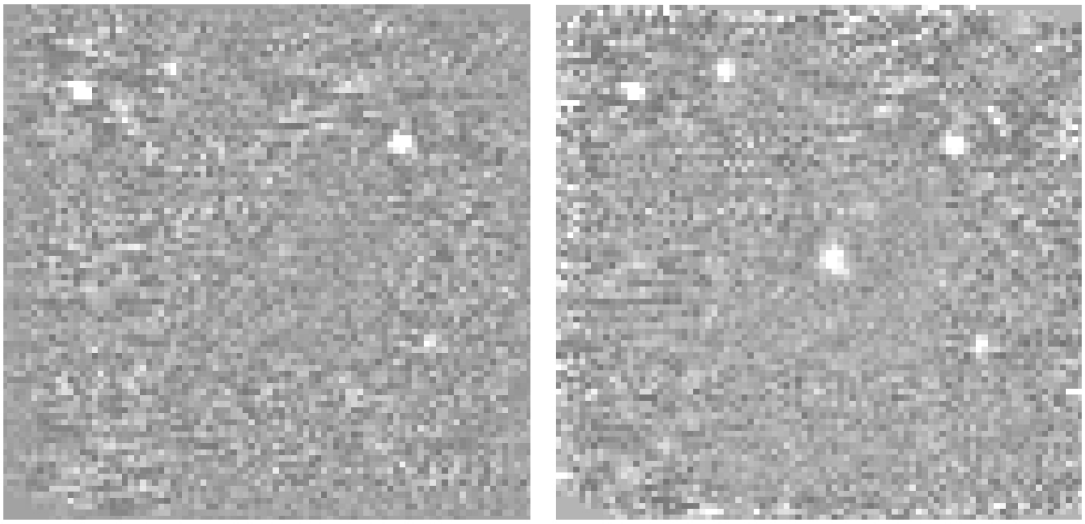

FIG. 10.—Two-dimensional reconstructed image of the cluster MRC 1022–299 obtained by integrating over the 5800–8000 Å wavelength range (*left*) and over 100 Å centered on the radio galaxy [O II] λ3727 emission line (*right*) redshifted at ≃7100 Å (redshift $z = 0.9085$). The radio galaxy O II emission is clearly extended and asymmetric, and a velocity field can be retrieved from the three-dimensional cube. In these images, east is up and north is to the right. About 3% of the pixels correspond to black/dead fiber spectra and have been cleaned with the IRAF task FIXPIX.

This research has been developed within the framework of the VVDS consortium. This work has been partially supported by the CNRS-INSU and its Programme National de Cosmologie (France), and by Italian Ministry (MIUR) grants COFIN2000 (MM02037133) and COFIN2003 (2003020150). This work has been partly supported by the Euro3D Research Training Network. The VLT VIMOS observations have been carried out during guaranteed time (GTO) allocated by the European Southern Observatory (ESO) to the VIRMOS consortium, under a contractual agreement between the Centre National de la Recherche Scientifique of France, heading a consortium of French and Italian institutes, and ESO, to design, manufacture, and test the VIMOS instrument.

REFERENCES

Allington-Smith, J., & Content, R. 1998, PASP, 110, 1216
Allington-Smith, J., et al. 2002, Exp. Astron., 13, 1
Bacon, R., et al. 1995, A&AS, 113, 347
———. 2001, MNRAS, 326, 23
Bonneville, C., et al. 2003, Proc. SPIE, 4841, 1771
Chapman, S. C., McCarthy, P. J., & Persson, S. E. 2000, AJ, 120, 1612
Content, R. M., et al. 2000, Proc. SPIE, 4013, 851
Emsellem, E., et al. 2004, MNRAS, 352, 721
Horne, K. 1986, PASP, 98, 609
Le Fèvre, O., et al. 2002, Messenger, 109, 21
McCarthy, P. J., Kapahi, V. K., van Breugel, W. Persson, S. E., Athreya, R., & Subrahmanya, C. R. 1996, ApJS, 107, 19
Prieto, E., Le Fèvre, O., Saisse, M., Voet, C., & Bonneville, C. 2000, Proc. SPIE, 4008, 510
Scodeggio, M., et al. 2005, PASP, 117, 1284